ELSEVIER

Materials Science and Engineering B 121 (2005) 2–8

MATERIALS SCIENCE & ENGINEERING B

www.elsevier.com/locate/mseb

Preparation, characterization, ac conductivity and permittivity studies on vitreous $M_4AlCdP_3O_{12}$ (M = Li, Na, K) system

C.R. Mariappan [a], G. Govindaraj [a,*], S. Vinoth Rathan [a], G. Vijaya Prakash [b,1]

[a] *Department of Physics, School of Physical, chemical and Applied Sciences, Pondicherry University, R.V. Nagar, Kalapet, Pondicherry 605 014, India*
[b] *School of Physics and Astronomy, University of Southampton Highfield, Southampton S017 1BJ, UK*

Received 16 October 2004; accepted 12 November 2004

Abstract

Vitreous $M_4AlCdP_3O_{12}$ (M = Li, Na, K) NASICON-type materials are synthesized, characterized and their electrical properties are reported at different temperatures in the frequency range of 42 Hz to 1 MHz. Ac conductivity and permittivity data are analyzed by using conductivity formalism. The dc conductivity and hopping frequency are thermally activated and their activation energies found to be in the range of 0.79–0.85 eV. The variation of dielectric permittivity with frequency is attributed to ion diffusion and polarization occurring in the NASICON-type vitreous materials. Scaling in conductivity and permittivity shows that the relaxation mechanisms are independent of temperature for the NASICON-type vitreous materials.

Keywords: Amorphous materials; Electrical measurement; Ionic conduction; Polarization effects; Permittivity; Relaxation mechanism; Scaling analysis

1. Introduction

The discovery of Na^+-superionic conductors (NASICONs) $Na_{1+x}Zr_2Si_xP_{3-x}O_{12}$ represents an important improvement in solid electrolyte developments because their three-dimensional framework structure with high ionic conductivity comparable to that of two-dimensional networks, such as β-alumina [1]. Numerous NASICON-related phosphate materials are prepared and their ionic conductivity has been reported [2–11]. The great stability of the tetrahedral oxyanions $(PO_4)^{3-}$ gives phosphates a remarkable structural diversity in the case of monophosphates for which the atomic structure results from the Coulomb attraction between independent cations and oxyanions. The general formula of NASICON materials is $M_xB_yP_3O_{12}$, where M is an alkali ion and B is one or more ions in tri-, tetra-, or penta-valent state. The NASICON materials is built up of $B_y(PO_4)_3$ units in which two BO_6 octahedra are linked to three PO_4 tetrahedra by shared oxygens. During the past few years, particular attention has been paid to combine titanium and aluminum-based different materials with NASICON structure due to high ionic conductivity. The high conductivity value 0.7×10^{-3} S/cm at room temperature is obtained for the $Li_{1+x}Al_xTi_{2-x}P_3O_{12}$ for $x = 0.3$, and $Li_{1+x}Al_xGe_yTi_{2-x-y}P_3O_{12}$ for $x = 0.5$ and $y = 0.8$. These are amongst the highest value reported so far [2,7,12]. However, the applicability as solid electrolyte is limited by a possible Ti^{4+}/Ti^{3+} reduction in contact with anodes and by large grain boundary contribution. The above drawbacks can be removed (i) by avoiding Ti in the preparation and (ii) the vitrification of NASICON compositions.

Further, it is interesting to know the ability to vitrification for NASICON compounds and to examine the ionic conduction and relaxation mechanism. The primary source of experimental electrical information regarding the relaxation mechanism has been derived from frequency dependent dielectric spectroscopy. Measurement of frequency dependent conductivity and permittivity not only provide for information on the steady state transport, but also reflect at high frequency transient dielectric response resulting from localized displacement of the ions [13,14].

* Corresponding author. Tel.: +91 413 2655991x405; fax: +91 413 2655255.
E-mail address: ggraj_7@yahoo.com (G. Govindaraj).
[1] Present address: Department of Physics, Indian Institute of Technology, New Delhi 110016, India.

0921-5107/$ – see front matter © 2004 Elsevier B.V. All rights reserved.
doi:10.1016/j.mseb.2004.11.005

In the present paper, we report the synthesis, characterization and relaxation mechanism in $M_4AlCdP_3O_{12}$ (M = Li, Na, K) aluminum-based NASICON-type vitreous materials. Ac conductivity and permittivity are analyzed by using conductivity formalism. We also present the time temperature superposition principle (TTSP) of conductivity and permittivity spectra at different temperatures for given NASICON-type sample and for various alkali ions present in NASICON-type vitreous materials at arbitrary temperature.

2. Experiment

The vitreous materials $Li_4AlCdP_3O_{12}$ (LACP), $Na_4AlCdP_3O_{12}$ (NACP) and $K_4AlCdP_3O_{12}$ (KTCP) were prepared by a solid-state reaction from Li_2CO_3, Na_2CO_3, K_2CO_3, Al_2O_3, CdO, $NH_4H_2PO_4$. The LACP system was prepared by taking stochiometric quantities of Li_2CO_3, Al_2O_3, CdO, $NH_4H_2PO_4$ and these were heated. The overall reaction for the formation of LACP is given by:

$$2Li_2CO_3 + \tfrac{1}{2}Al_2O_3 + CdO + 3NH_4H_2PO_4 \xrightarrow{\Delta}$$
$$Li_4AlCdP_3O_{12} + 3NH_3 + \tfrac{9}{2}H_2O + 2CO_2$$

The procedure followed in the synthesis of samples are: (i) the calculated amounts of the starting materials were ground in an agate mortar for 45 min; (ii) the mixture was placed in silica crucible and slowly heated in an electrical furnace up to 523 K and further heated and held at a temperature of 623 K for 6 h in order to ensure the total decomposition of the reagents; (iii) after cooling the sample to room temperature, the mixture was again ground for 45 min in agate mortar and heated in a silica crucible for ∼16 h at temperature 973–1073 K without melting the mixtures; (iv) the sample was heated further to temperatures of 1273–1373 K and the sample was melted at these temperature range and stirred 5–10 min to ensure homogeneity; (v) finally, the melt was poured into stainless steel plate and quenched by pressing with another stainless steel plate at room temperature.

X-ray powder diffraction (XRPD) patterns were recorded for all the compounds using the Rigaku miniflex X-ray diffractometer with monochromatic Cu Kα radiation at glancing angles between 5 and 65°. Fourier transform infrared (FT-IR) spectra were recorded in the wave number range of 1600–400 cm^{-1} using Shimadzu FTIR–8700 Fourier transform infrared spectrophotometer by KBr pellet method at room temperature and 40 scans at 4 cm^{-1} resolution were averaged. The density of the vitreous material bits free of air bubbles and cracks on visual examination was determined by the Archimede's principle with toluene as an inert immersion liquid. The error in the density measurement is within ± 0.04 gm/cm^3. Differential scanning calorimetry was performed for all the samples on a Mettler Toledo DSC 821^e instrument. The temperature was varied from 308 to 798 K at a heating rate of 10 K/min.

The samples for electrical conductivity measurements were made by cutting the prepared vitreous samples ∼10 mm diameter and ∼1.5–2.0 mm thickness. Both sides of the samples were ground and polished by using silicon carbide plate and silicon carbide powder (mesh size 1200) with water as free lubricant. Then the samples were washed in flow water. Immediately the washed samples were heated slowly up to 423 K and held at this temperature for 1 h to remove the water on sample surface. Silver paint was pasted on parallel surface of the polished sample. Measurements were performed in vacuum atmosphere. Spring loaded contacts were connected the silver plates of the sample to the input ports of a commercial Hioki 3532-50 LCR Hitester which together with a dedicated computer and software acquired measurements of the parallel conductance (G) and capacitance (C) of the material as a function of frequency range of 42 Hz to 1 MHz at different temperatures.

3. Results and discussion

The amorphous nature of the NASICON-type samples was confirmed by XRPD studies and the results are shown in Fig. 1(a). Fig. 1(b) shows the FT-IR absorption spectra observed for the different NASICON-type vitreous materials. The entire region down to 400 cm^{-1} is dominated by the vibrations of the PO_4 tetrahedra and these features are same in all samples. Table 1 shows the FT-IR absorption bands and their attribution of NASICON-type vitreous samples are assigned to various vibrational contributions of the basic phosphates [15–20]. Further, FT-IR spectra show the absence of carbonates related IR peaks in the region 1400–1500 cm^{-1}, suggesting fully vitrified composition. Density of the samples found by using Archimede's principle and it is used to calculated the molar volume $V_m = M/\rho$, where M is the corresponding molecular weight of the samples (Table 2).

The DSC thermogram was recorded for all the samples and it is shown in Fig. 1 (c) at scan rate of 10 K/min. The endothermic peak and exothermic peaks observed in the DSC are corresponds to the glass transition and crystallization respectively for the present amorphous material. The glass transition (T_g) and crystallization temperatures (T_c) of all vitreous samples are shown in Table 2. It is to be noted that the sample NACP shows two exothermic peaks related to the crystallization temperatures (T_{c1} and T_{c2}). Relatively high glass transition temperatures suggesting thermal durability of the present glasses.

3.1. Ac conductivity studies

The measured parallel conductance (G) data were converted with appropriate geometric factor to find the frequency dependent conductivity $\sigma(\omega)$. Ac conductivity for KACP is shown in Fig. 2, as an example. The conductivity ($\sigma(\omega)$) is found to be frequency independent in the lower frequency region ($\omega < \omega_p$), suggesting that the ionic diffusion is random

Table 1
FT-IR absorption bands for the NASICON-type vitreous materials

Sample	Harmonics of O–P–O bending	O–P–O asymmetric bending	P–O–P stretching	Ionic group PO_4^{3-}
LACP	413	574	731	949, 1074
NACP	444	550	719	1069, 1092
KACP	424	555	729	940, 1057

FT-IR absorption maxima (in cm^{-1}).

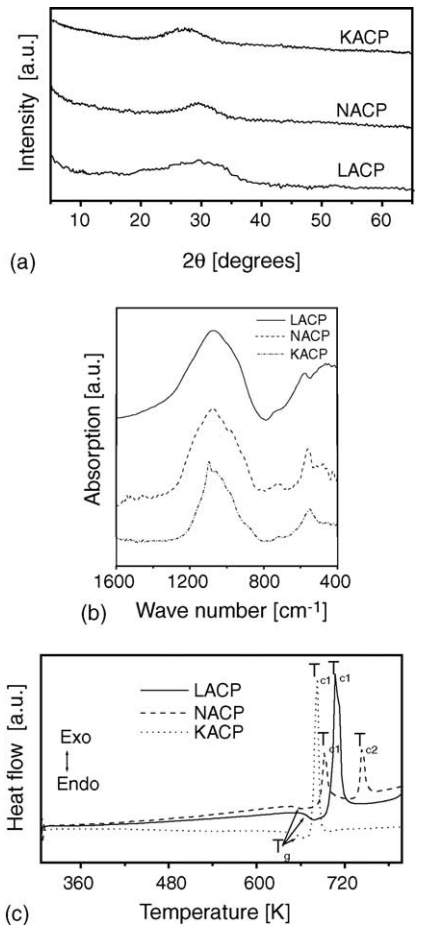

Fig. 1. . (a) XRPD spectra for $Li_4AlCdP_3O_{12}$ (LACP), $Na_4AlCdP_3O_{12}$ (NACP), and $K_4AlCdP_3O_{12}$ (KACP) samples. (b) FT-IR spectra of NASICON type samples. (c) DSC thermogram of NASICON-type materials.

less, i.e. the ions perform correlated forward-backward motions [21]. While the frequency exceeds hopping frequency ω_p, $\sigma(\omega)$ increases with frequency following power law dispersion $\sigma(\omega) \propto \omega^n$, (where $n < 1$). The ac conductivity behavior is analyzed by using conductivity formalism i.e. universal power law (UPL) [13,22]:

$$\sigma(\omega) = \sigma_{dc} + A\omega^n = \sigma_{dc}\left[1 + \left(\frac{\omega}{\omega_p}\right)^n\right] \quad (1)$$

Ac conductivity spectra for different temperatures are fitted to Eq. (1) and the parameters σ_{dc}, ω_p and n are extracted from the analysis. Continuous lines in Fig. 2 represent the UPL fit at different temperatures and similar results are obtained for other samples. The frequency exponent 'n' is found to be about 0.63 and is independent of temperature as well as composition. In general σ_{dc} and ω_p parameters show strongly temperature dependent. Such dependence is fitted with the Arrhenius equations

$$\sigma_{dc}T = \sigma_0 \exp\left(-\frac{E_\sigma}{kT}\right), \quad (2)$$

$$\omega_p = \omega_0 \exp\left(-\frac{E_p}{kT}\right), \quad (3)$$

where σ_0 is the dc conductivity pre-exponential factor, k the Boltzmann's constant, E_σ the dc conductivity activation energy for mobile ions, ω_0 the pre-exponential of hopping frequency, E_p, the activation energy for hopping frequency. Fig. 3(a) and (b) show the Arrhenius plots for σ_{dc} and ω_p, respectively. Both of these parameters show strong

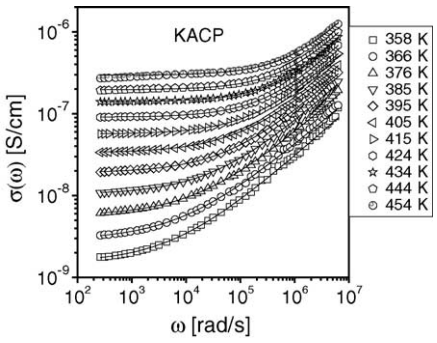

Fig. 2. Ac conductivity of KACP at different temperatures. The solid lines are the fits to Eq. (1).

Table 2
Density (ρ), molar volume (V_m), glass transition temperature (T_g), crystallization temperatures (T_{c1}, T_{c2}), frequency exponent (n), dc conductivity activation energy (E_σ), hopping frequency activation energy (E_p), ac conductivity activation energy (E_a), dielectric loss strength ($\Delta\varepsilon$) and many particle crossover length ($\langle R^2\rangle_{cr}$) for the NASICON-type vitreous samples

Sample	ρ (gm/cm^3)	V_m (cm^3)	T_g (K)	T_{c1}, T_{c2} (K)	$T_{c1}-T_g$ (K)	n ±0.03	E_σ (eV) ±0.02	E_p (eV) ±0.03	E_a (eV) ±0.02	$\Delta\varepsilon$	$\langle R^2\rangle_{cr}$ (Å)
LACP	2.71	166.82	402	435	33	0.63	0.81	0.79	0.30	3.43	0.99
NACP	3.12	165.47	388	420, 471	32	0.63	0.85	0.83	0.31	4.36	1.05
KACP	2.41	240.95	389	409	20	0.63	0.78	0.79	0.29	3.38	0.90

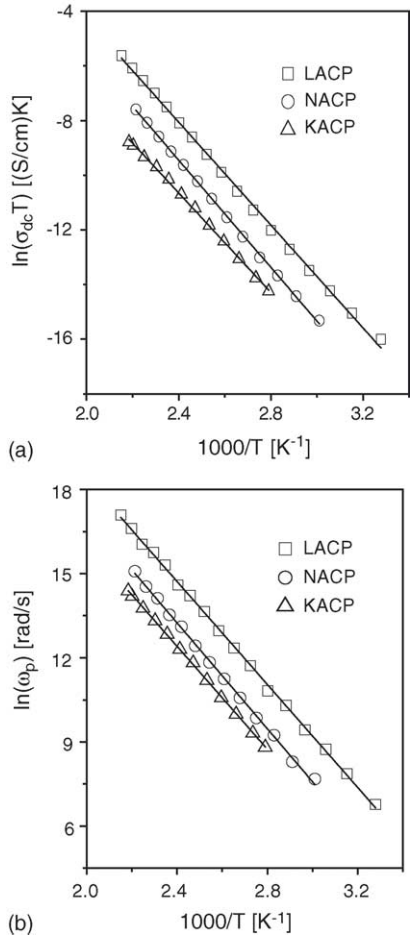

Fig. 3. (a) Arrhenius plots of dc conductivity for NASICON-type vitreous materials. The solid lines are the fits to Eq. (2). (b) Reciprocal temperature dependence of the hopping frequency for NASICON type samples. The continuous lines are the fits to Eq. (3).

correlation with the temperature with the general trend of LACP > NACP > KACP. These features suggest strong M-site alkali ion radius dependence and possible thermally-activated drift mobility of ions according to hopping mechanism [22]. Activation energies, E_σ, and E_p, thus derived from the fitting are shown in Table 2. It is also to be noted that the activation energies, E_p and E_σ are very close to each other, within the experimental error. This indicates that the charge carrier have to over come the same energy barrier while conducting as well as relaxing. Further, the ac conductivity activation energy E_a is calculated by using $E_a = (1-n)E_\sigma$ and is also tabulated in Table 2. The ac activation energy follows the trend of KACP < LACP and NACP. A similar experimental situation has been reported for alkali ion migration barriers in silicates, M_2O–$2SiO_2$ (M = Na, K) and binary NASICON-type glasses $M_3Fe_2P_3O_{12}$, $M_3Ga_2P_3O_{12}$, $M_4NbP_3O_{12}$ (M = Li, Na, K) [23,24].

We also evaluated the physical parameters, the dielectric loss strengths [25] ($\Delta\varepsilon$) and many-particle crossover lengths [26] ($\langle R^2\rangle_{cr}$) to give further emesis to our studies. Both these

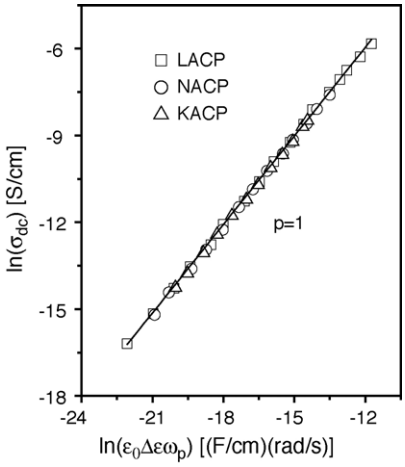

Fig. 4. $\ln(\sigma_{dc})$ vs. $\ln(\varepsilon_0\Delta\varepsilon\omega_p)$ plots for the NASICON-type materials. The solid line is a fit to Eq. (4) with $p = 1$.

parameters show lower values for KACP, similar to the trends shown by activation energies (Table 2).

Subsequently, to examined the correlation between the ac and dc conduction, we followed the Barton, Nakajima, and Namikawa (BNN) relation, where the following equation is to be valid for the most of the ion conducting materials [27]

$$\sigma_{dc} = p\varepsilon_0\Delta\varepsilon\omega_p, \tag{4}$$

where p is a numerical constant expected to be in the order of 1. Slope of the plot in Fig. 4 is equal to unity, implies that the dc and ac conductions are finely correlated and further suggesting that they follow the same mechanisms for different NASICON-type vitreous materials.

3.2. Ac permittivity studies

The imaginary part of the complex dielectric permittivity ε'' is obtained from Eq. (1) as

$$\varepsilon''(\omega) = \frac{[\sigma(\omega) - \sigma_{dc}]}{\varepsilon_0\omega} = \left(\frac{A}{\varepsilon_0}\right)\omega^{-(1-n)}, \tag{5}$$

while the real part ε' is given by:

$$\varepsilon'(\omega) = \varepsilon_\infty + \left(\frac{A}{\varepsilon_0}\right)\tan\left(\frac{n\pi}{2}\right)\omega^{-(1-n)}, \tag{6}$$

where ε_∞ is the high frequency value of $\varepsilon'(\omega)$. The measured capacitance (C) data were converted with appropriate geometric factor to find the real part of the dielectric permittivity $\varepsilon'(\omega)$ and the results are shown in Fig. 5 for KACP at different temperatures. We have fitted the $\varepsilon'(\omega)$ data at different temperatures to Eq. (6) using the magnitudes of n and $A = (\sigma_{dc}/\omega_p^n)$, obtained from the ac conductivity analysis [23]. In the high frequency region, at low temperatures, the well-known non-Debye behavior $\omega^{(n-1)}$ is observed [13,28]. However, in the low frequency region, at high temperatures, the sharp increase is due to the contribution from the charge accumulation at the electrode-sample interface. At high fre-

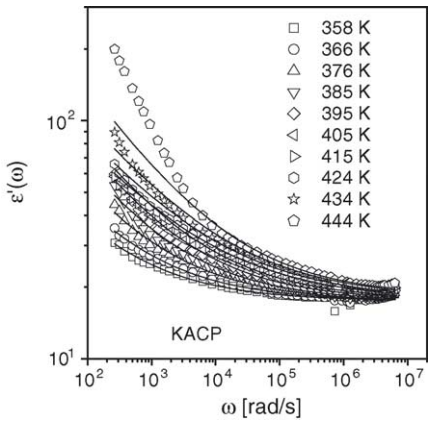

Fig. 5. Real part of permittivity vs. frequency at selected temperatures for KACP. The continuous lines are the fits to Eq. (6).

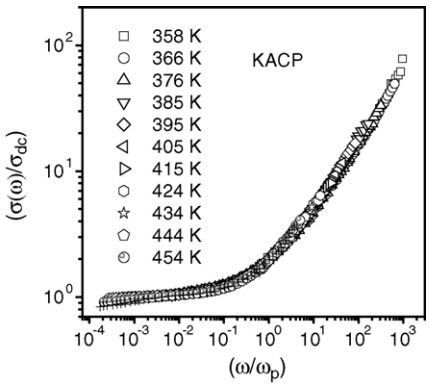

Fig. 6. Scaling plots for the conductivity spectra in Fig. 2. The conductivity and frequency axes are scaled by the dc conductivity and hopping frequency, respectively.

quencies, due to the high periodic reversal of the field at the interface, the contribution from charge carriers towards the dielectric constant decreases with increasing frequency [28]. Hence, $\varepsilon'(\omega)$ is found to decrease with increasing frequency.

3.3. Ac conductivity scaling

Ion dynamic process in ion conducting materials has been the subject of intense scientific interest for the past several years [29]. The ac conductivity is a direct evidence for the ion dynamic process in solids and the study of the conductivity spectra in disordered solids at different temperatures leads to a scaling law and it is called the time-temperature superposition principle (TTSP) [29]. This means, for a given material, the conductivity isotherms can be collapsed into a single curve with appropriate scaling of the conductivity and frequency axis. This feature can be expressed by:

$$\frac{\sigma(\omega)}{\sigma_{dc}} = F_1\left(\frac{\omega}{\omega_c}\right), \tag{7}$$

where F_1 is a temperature-independent function and ω_c is a temperature dependent characteristic frequency. Various workers have considered the dc conductivity σ_{dc} as a scaling factor for the ac conductivity axis and the characteristic frequency ω_c as a scaling parameter for the frequency axis [29–31].

We have studied the ac conductivity scaling by choosing the characteristic frequency $\omega_c = \omega_p$. The scaled conductivity spectra are shown in Fig. 6 for KACP at different temperatures, where the conductivity axis is scaled by σ_{dc}, and the frequency axis by ω_p. The scaled ac conductivity data are collapsed into a single curve. Obviously, the TTSP is fulfilled and suggesting the conductivity relaxation mechanism is independent of temperatures. Similar scaling results are observed for other glasses. Conductivity master plot for different glasses are shown in Fig. 7, where the conductivity axis is scaled by σ_{dc}, and frequency axis by ω_p at arbitrary temperatures. The scaled ac conductivity data are superimposed into a single master curve. Obviously, the TTSP is fulfilled and suggesting the conductivity relaxation mechanism is independent of various alkali ions present in the NASICON-type vitreous samples.

3.4. Permittivity scaling studies

The real part of permittivity increases with decreasing frequency and approaches a limiting value ε_s at low frequencies associated with the polarization resulting from alignment of the dipoles along the direction of the electric field. For ion conducting glasses the mobile ions and oppositely charged matrix are assumed as dipoles. In ion conducting glasses polarization and conduction process are integrated into a single and continuous process [25].

Scaling behavior is also investigated for the real part of permittivity of NASICON-type samples by using the relation,

$$\frac{(\varepsilon'(\omega) - \varepsilon_\infty)}{\Delta\varepsilon} = F_2\left(\frac{\omega}{\omega_p}\right), \tag{8}$$

where ε_∞ is the dielectric permittivity at high frequency, $\Delta\varepsilon$ the dielectric loss strength, F_2 the temperature indepen-

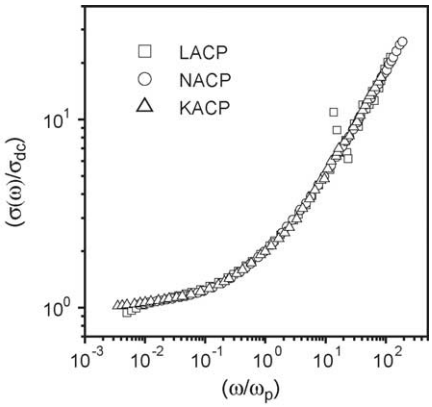

Fig. 7. Ac conductivity master curves for different NASICON-type vitreous materials at arbitrary temperature. The conductivity and frequency axes are scaled by the dc conductivity and hopping frequency, respectively.

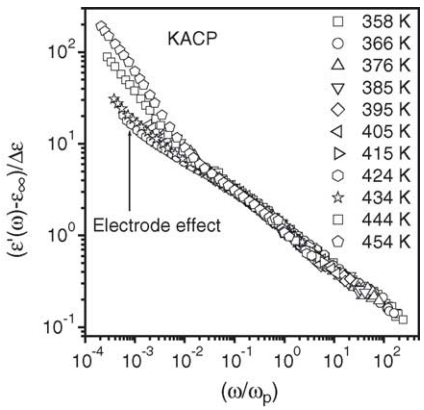

Fig. 8. Scaled ac permittivity spectra for KACP at different temperatures according to Eq. (8).

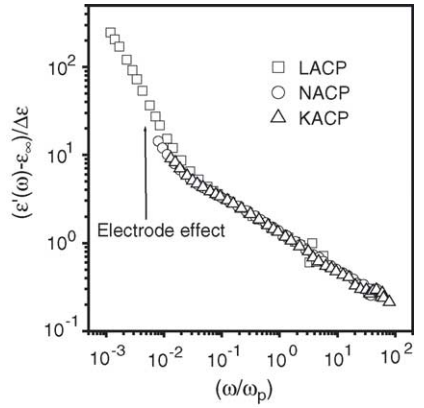

Fig. 9. Ac permittivity master plot for different NASICON-type samples at arbitrary temperature according to Eq. (8).

dent function, and ω_p the temperature dependent hopping frequency.

The scaled permittivity spectrum is shown in Fig. 8 for KACP at different temperatures, where the ac permittivity is subtracted by dielectric constant, ε_∞, and then scaled by dielectric loss strength, $\Delta\varepsilon$ and the frequency axis scaled by ω_p. In Fig. 9, frequency axis is scaled by ω_p for different NASICON-type samples at arbitrary temperature. The scaled ac permittivity data of NASICON-type materials are superimposed into a single curve, except in the lower frequency region where the electrode effects are prominent. This study suggests that the permittivity relaxation mechanism is independent of temperatures and the compositional variation in the NASICON-type vitreous materials.

4. Conclusions

The NASICON-type vitreous materials: $M_4AlCdP_3O_{12}$ (M = Li, Na, K) are successfully prepared and further characterized by using XRPD, DSC, and FT-IR. Electrical properties of these materials were studied over a wide range of temperature and frequency. Conductivity formalism is used to evaluate various important parameters, namely dc conductivity, the hopping frequency, and dielectric loss strength. Crystallization temperature, dc conductivity and hopping frequency are found to be increasing with the decrease of alkali ionic radius of M site. The BNN relation confirms that the ac and dc conduction mechanism are successfully correlated. Scaling studies of conductivity and the permittivity spectra further appreciates the merit of our systems, and also shows generalized features of other reported ionic crystalline materials and glasses.

Acknowledgments

The financial support from CSIR and AICTE, Government of India, research projects F. 03/0973/02 EMR-II and F. 8019/RDII/MOD/MAT(95)/2000-01 are gratefully acknowledged for this work. One of us (C.R.M) would like to thank the Council of Scientific and Industrial Research, Government of India, for the award of a Senior Research Fellowship. We are indebted to Dr. Bernhard Roling for his help in theoretical calculations.

References

[1] H.Y.-P. Hong, Mater. Res. Bull. 11 (1976) 173;
J.B. Goodenough, H.Y.-P. Hong, J.A. Kafalas, Mater. Res. Bull. 11 (1976) 203.
[2] K. Arbi, S. Mandal, J.M. Rojo, J. Sanz, Chem. Mater. 14 (2002) 109.
[3] F. d'Yvoire, M. Pintard-Screpel, E. Bretey, M. de le Rochere, Solid State Ionics 9/10 (1983) 851.
[4] Ph. Colomban, Solid State Ionics 21 (1986) 97.
[5] L. Moreno-Real, P. Maldonado-Manso, L. Leon-Reina, E.R. Losilla, F.E. Mouahid, M. Zahir, J. Sanz, J. Mater. Chem. 12 (2002) 3681.
[6] J. Alamo, R. Roy, J. Mater. Sci. 21 (1986) 444.
[7] H. Aono, E. Sugimoto, Y. Sadaoka, N. Imanaka, G. Adachi, J. Electrochem. Soc. 137 (1990) 1023.
[8] A. El Jazouli, C. Parent, J.M. Dance, G. Le Flem, P. Hagenmuller, J.C. Viala, J. Solid State Chem. 74 (1988) 377.
[9] C.R. Mariappan, G. Govindaraj, Mater. Sci. Eng. B 94 (2002) 82.
[10] G. Govindaraj, C.R. Mariappan, Solid State Ionics 147 (2002) 49.
[11] S. Barth, R. Olazcuaga, P. Gravereau, G. Le Flem, P. Hagenmuller, Mater. Lett. 16 (1993) 96.
[12] P. Maldonado-Manso, E.R. Losilla, M. Martinez-Lara, M.A.G. Aranda, S. Bruque, F.E. Mouahid, M. Zahir, Chem. Mater. 15 (2003) 1879.
[13] A.K. Jonscher, Dielectric Relaxation in Solids, Chelsea Dielectric Press, London, 1983.
[14] D.L. Sidebottom, C.M. Murray-Krezan, Phys. Rev. Lett. 89 (2002) 195901.
[15] A.A. Higazy, B. Bridge, J. Mater. Sci. 20 (1985) 2345.
[16] K. Nakamoto, Infrared Raman Spectra of Inorganic and Coordination Compounds: Part A. Theory and Applications in Inorganic Chemistry, Wiley, New York, 1997.
[17] C. Dayanand, G. Bhikshamaiah, V. Jayatyagaraju, M. Salagram, A.S.R. Krishnamurthy, J. Mater. Sci. 31 (1996) 1945.
[18] I.N. Chakraborty, R.A. Condrate Snr, Phys. Chem. Glasses 26 (1985) 68.
[19] D.E.C. Corbridge, E.J. Lowe, J. Chem. Soc. Part I (1954) 493.

[20] K.J. Rao, K.C. Sobha, S. Kumar, Proc. Ind. Acad. Sci. 113 (2001) 497.
[21] K. Funke, Prog. Solid State Chem. 22 (1993) 111.
[22] D.P. Almond, G.K. Duncan, A.R. West, Solid State Ionics 9/10 (1983) 277;
D.P. Almond, G.K. Duncan, A.R. West, J. Non-Cryst. Solids 74 (1985) 285;
D.P. Almond, A.R. West, R. Grant, Solid State Commun. 44 (1982) 1277.
[23] G.N. Greaves, S.J. Gurman, C.R.A. Catlow, A.V. Chadwick, S. Houde-Walter, C.M.B. Henderson, B.R. Dolson, Phil. Mag. A 64 (1991) 1059.
[24] K.C. Shobha, K.J. Roa, J. Non-Cryst. Solids 201 (1996) 52.
[25] D.L. Sidebottom, J. Zhang, Phys. Rev. B 62 (2000) 5503.
[26] B. Roling, C. Martiny, S. Bruckner, Phys. Rev. B 63 (2001) 214203.
[27] J.C. Dyre, J. Non-Cryst. Solids 88 (1986) 271.
[28] J.R. Macdonald (Ed.), Impedance Spectroscopy, Wily, New York, 1987.
[29] J.C. Dyre, T.B. Schrøder, Rev. Mod. Phy. 72 (2000) 873, reference therein.
[30] B. Roling, Phys. Chem. Chem. Phys. 3 (2001) 5093.
[31] S. Murugavel, B. Roling, Phys. Rev. Lett. 89 (2002) 079602;
S. Murugavel, B. Roling, Phys. Rev. Lett. 89 (2002) 195902.